Elucidating the Specificity of Binding of Sulfonylurea Herbicides to Acetohydroxyacid Synthase†

Jennifer A. McCourt, Siew Siew Pang,‡ Luke W. Guddat,* and Ronald G. Duggleby

Department of Biochemistry and Molecular Biology, The University of Queensland, Brisbane, Queensland 4072, Australia

Received September 19, 2004; Revised Manuscript Received November 22, 2004

ABSTRACT: Acetohydroxyacid synthase (AHAS, EC 2.2.1.6) is the target for the sulfonylurea herbicides, which act as potent inhibitors of the enzyme. Chlorsulfuron (marketed as Glean) and sulfometuron methyl (marketed as Oust) are two commercially important members of this family of herbicides. Here we report crystal structures of yeast AHAS in complex with chlorsulfuron (at a resolution of 2.19 Å), sulfometuron methyl (2.34 Å), and two other sulfonylureas, metsulfuron methyl (2.29 Å) and tribenuron methyl (2.58 Å). The structures observed suggest why these inhibitors have different potencies and provide clues about the differential effects of mutations in the active site tunnel on various inhibitors. In all of the structures, the thiamin diphosphate cofactor is fragmented, possibly as the result of inhibitor binding. In addition to thiamin diphosphate, AHAS requires FAD for activity. Recently, it has been reported that reduction of FAD can occur as a minor side reaction due to reaction with the carbanion/enamine of the hydroxyethyl−ThDP intermediate that is formed midway through the catalytic cycle. Here we report that the isoalloxazine ring has a bent conformation that would account for its ability to accept electrons from the hydroxyethyl intermediate. Most sequence and mutation data suggest that yeast AHAS is a high-quality model for the plant enzyme.

The sulfonylurea herbicides were discovered in an extensive synthetic and screening program led by Levitt and colleagues (*1*). The general features of most active compounds (Figure 1) are an aromatic ring attached to the sulfur atom of the sulfonylurea bridge and a heterocyclic ring attached to the distal nitrogen atom. The aromatic ring is *ortho*-substituted, while the heterocyclic ring, which is either a pyrimidine (X = CH) or triazine (X = N), is substituted in both *meta* positions.

It was not until several years after the introduction of sulfonylureas that the molecular basis of their herbicidal activity was established (*2*, *3*). They inhibit acetohydroxyacid synthase (AHAS,[1] EC 2.2.1.6), the enzyme that catalyzes the first common step in branched chain amino acid biosynthesis [see the review by Duggleby and Pang (*4*)]. Nevertheless, the mechanism of inhibition of AHAS has only been understood in the past few years by determining the crystal structure of yeast AHAS, first without (*5*) and then with chlorimuron ethyl (CE; see Figure 1) bound (*6*). The active site is located at the bottom of a deep hydrophobic tunnel; CE is inserted into the entrance of this tunnel with the heterocyclic ring projecting toward the active site, while the aromatic ring is bound in a pocket near the surface of the protein. The herbicide makes multiple interactions with amino acid side chains in the active site tunnel, and mutation of most of these residues results in resistance to CE and other sulfonylureas (*7*).

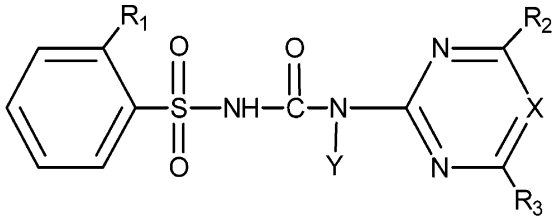

Herbicide	R_1	R_2	R_3	X	Y
Chlorimuron ethyl (CE)	$CO\text{-}OC_2H_5$	OCH_3	Cl	CH	H
Chlorsulfuron (CS)	Cl	OCH_3	CH_3	N	H
Sulfometuron methyl (SM)	$CO\text{-}OCH_3$	CH_3	CH_3	CH	H
Metsulfuron methyl (MM)	$CO\text{-}OCH_3$	OCH_3	CH_3	N	H
Tribenuron methyl (TB)	$CO\text{-}OCH_3$	OCH_3	CH_3	N	CH_3

FIGURE 1: Structures of sulfonylurea herbicides.

† This work was supported by Grants A00105313 and DP0450275 from the Australian Research Council to R.G.D. and L.W.G. The use of the BioCARS sector was supported by the Australian Synchrotron Research Program, which is funded by the Commonwealth of Australia under the Major National Research Facilities Program. Use of BioCARS Sector 14 was also supported by the National Institutes of Health, National Center for Research Resources, under Grant RR07707. Use of the Advanced Photon Source was supported by the U.S. Department of Energy, Basic Energy Sciences, Office of Energy Research, under Contract W-31-109-Eng-38.

* To whom correspondence should be addressed. E-mail: luke.guddat@uq.edu.au. Telephone: 61 (07) 3365 3549. Fax: 61 (07) 3365 4699.

‡ Present address: Novartis Institute for Tropical Diseases, 10 Biopolis Road, #05-01, Chromos, Singapore 138670.

[1] Abbreviations: AHAS, acetohydroxyacid synthase; CE, chlorimuron ethyl; CS, chlorsulfuron; MM, metsulfuron methyl; SM, sulfometuron methyl; TB, tribenuron methyl; ThDP, thiamine diphosphate; YF1, 2,5-dimethyl-5,6-dihydropyrimidin-4-amine; YF3, 2-{[(6-amino-2-methyl-4,5-dihydropyrimidin-5-yl)methyl]amino}propane-1-thiol; YF4, 5-{[ethyl(methyl)amino]methyl}-2-methyl-5,6-dihydropyrimidin-4-amine; NSP, 5-(aminomethyl)-2-methyl-5,6-dihydropyrimidin-4-amine; P22, ethyl diphosphate; P23, propyl diphosphate; P25, pentyl diphosphate.

10.1021/bi047980a CCC: $30.25
Published on Web 01/28/2005

The sensitivity of AHAS to the different sulfonylureas varies substantially. For example, of the five sulfonylureas shown in Figure 1, the inhibition constants for yeast AHAS (*7*) range from 3.25 nM for CE to 127 nM for chlorsulfuron (CS). Moreover, the effect of active site tunnel mutations varies widely between these inhibitors. Thus, the G116S mutation in yeast AHAS increases the inhibition constant for CE by more than 1000-fold, while that for CS is increased by less than 5-fold. These observations suggest that the interactions with the protein must differ among various sulfonylureas. For this reason, we have now determined the structure of yeast AHAS with bound CS, sulfometuron methyl (SM), metsulfuron methyl (MM), and tribenuron methyl (TB).

The reaction catalyzed by AHAS involves the initial decarboxylation of pyruvate, followed by the reaction of the enzyme-bound hydroxyethyl moiety with a 2-ketoacid to give an acetohydroxy acid. The second substrate may be either pyruvate or 2-ketobutyrate, yielding 2-acetolactate or 2-aceto-2-hydroxybutyrate, respectively. These are subsequently metabolized to yield valine and leucine from 2-acetolactate or isoleucine from 2-aceto-2-hydroxybutyrate. Like many enzymes that catalyze the decarboxylation of pyruvate or other 2-ketoacids, AHAS requires thiamine diphosphate (ThDP) as an essential cofactor. ThDP-dependent enzymes also require Mg^{2+} or another divalent cation to anchor ThDP to the protein through its diphosphate tail. A third cofactor requirement of AHAS, first reported 40 years ago (*8*), is for FAD. There is no intrinsic feature of the reaction catalyzed that demands this requirement, as is demonstrated by the fact that there is an FAD-independent form of the enzyme in some bacteria (*9*). The proposal that FAD in AHAS is an evolutionary remnant from an ancestral FAD-dependent pyruvate oxidase-like protein (*10*, *11*) was confirmed when our first AHAS structure was determined (*5*). The position and conformation of FAD are very similar to those observed in pyruvate oxidase (*12*). The hypothesis that FAD plays a purely structural role is supported by comparison of the structures of the FAD-dependent and FAD-independent enzymes (*13*).

Although there is no apparent catalytic role of FAD in AHAS, partial loss of the absorbance of FAD during AHAS catalysis was reported by Schloss and Aulabaugh (*14*). Very recently, a re-examination of this phenomenon (*15*, *16*) has established that FAD can undergo reduction to $FADH_2$ as a side reaction of the catalytic cycle by reacting with the carbanion/enamine of the enzyme-bound hydroxyethyl−ThDP intermediate to form acetyl ThDP. While the proximity of FAD to the active site might allow indirect electron transfer, the geometry of the isoalloxazine ring would not favor its reduction. In pyruvate oxidase, the isoalloxazine ring is bent by 15° across the N5−N10 axis to yield a conformation that is expected to increase its redox potential (*17*). In the previous AHAS structures, the isoalloxazine ring appears to be flat (*5*, *6*); therefore, $FADH_2$ formation would not be favored. However, the resolution of these structures (2.6 and 2.8 Å) may not have been sufficient to reveal a slight bend. In the new structures reported here, with resolutions to 2.19 Å, we now see that the isoalloxazine ring is bent in a way that is indistinguishable from that in pyruvate oxidase. Thus, these new data help in understanding how FAD reduction can occur.

MATERIALS AND METHODS

Protein Expression, Purification, Crystallization, and X-ray Data Collection. The catalytic subunit of yeast AHAS (*18*) was expressed and purified as described previously. The first 57 residues of yeast AHAS comprise a mitochondrial transit peptide that is not present in the mature protein; the DNA encoding this peptide was removed during cloning into the expression vector. The recombinant protein consists of a residual peptide containing a hexahistidine tag derived from the pET-30 expression vector, followed by residues 58−687 of AHAS. Residues are numbered according to the theoretical translation product of the yeast *ilv2* gene. AHAS activity was determined using published methods (*19*). Protein concentrations were estimated using the bicinchoninic acid protein determination kit (Sigma), based on the method of Smith et al. (*20*).

Crystals of yeast AHAS complexes were grown by hanging drop vapor diffusion in the presence of 1 mM ThDP, 1 mM $MgCl_2$, 1 mM FAD, 1 mM inhibitor, 5 mM DTT, 0.2 M potassium phosphate (pH 7.0), 0.1 M Tris-HCl (pH 7.0), 0.2 M Li_2SO_4, and 0.9 M sodium potassium tartrate. X-ray data (Table 1) were collected from cryoprotected crystals [equilibrated with 30% (v/v) ethylene glycol] at 100 K on beamline 14BMC at the Advanced Photon Source (Argonne National Laboratory, Argonne, IL). The data were indexed, integrated, and scaled using DENZO and SCALEPACK (*21*).

Structure Determination. The structures of the yeast AHAS complexes with CS, TB, and SM were determined by difference Fourier methods using the protein coordinates for the yeast AHAS−CE complex [Protein Data Bank (PDB) entry 1N0H]. The yeast AHAS−MM complex crystallized in a space group different from that of the other structures (*I*422 vs *P*422; Table 1); thus, molecular replacement was required for phasing. AMoRe (*22*) was used to determine the location of the two yeast AHAS dimers in the asymmetric unit. Refinement of all four structures was carried out using CNS (*23*) with model building and structure interpretation implemented by using O (*24*). The initial difference Fourier maps showed complete electron density for FAD and for the various herbicides. Broken density was observed for ThDP in all of the structures. The assignment of the structures of the fragmented pieces of ThDP is discussed in the Results and Discussion. The cofactors and inhibitors were subsequently built into the residual electron density. Refinement of the structures was completed by the inclusion of ordered water molecules, the assignment of individual *B*-factors for all atoms, and the inclusion of multiple conformations for some side chains. An overall anisotropic *B*-factor correction was applied using the standard protocol in CNS. The R_{factor} and R_{free} for all of the final structures and the model geometries are presented in Table 1. The coordinates and structure factors for the four complexes have been deposited with the Protein Data Bank as entries 1T9B, 1T9D, 1T9C, and 1T9A for the CS, MM, SM, and TB complexes, respectively. Figures were generated with SETOR (*25*), MOLSCRIPT (*26*), RASTER 3D (*27*), WebLab ViewerPro (MSI, San Diego, CA), and Chemsketch (ACD Labs, Toronto, ON).

RESULTS AND DISCUSSION

Overall Structures. Three of the complexes (with CS, SM, and TB) crystallized in space group *P*422 with a dimer as

Table 1: Data Collection, Refinement, and Structure Statistics for the Yeast AHAS−Herbicide Complexes

	CS	MM	SM	TB
crystal parameters				
unit cell lengths (Å) $a = b, c$	154.6, 178.8	218.3, 361.5	154.5, 178.8	154.6, 178.8
space group	*P*422	*I*422	*P*422	*P*422
crystal dimensions (mm)	0.5 × 0.2 × 0.2	0.5 × 0.2 × 0.2	0.4 × 0.2 × 0.2	0.3 × 0.2 × 0.2
diffraction data[a]				
temperature (K)	100	100	100	100
resolution range (Å)	50−2.19	50−2.29	50−2.34	50−2.58
no. of observations [$I > 0\sigma(I)$]	531345 (14583)	1407518 (83495)	816734 (50178)	517558 (20865)
no. of unique reflections [$I > 0\sigma(I)$]	102885 (5842)	160659 (12195)	90495 (7810)	67083 (5303)
completeness (%)	92.9 (53.4)	83.6 (64.0)	98.6 (86.6)	97.8 (78.6)
R_{sym}[b]	0.058 (0.219)	0.056 (0.254)	0.072 (0.262)	0.072 (0.253)
$\langle I\rangle/\langle\sigma(I)\rangle$	17.0 (4.1)	18.5 (5.7)	15.6 (8.5)	14.6 (6.0)
refinement				
resolution limits (Å)	50−2.19	50−2.29	50−2.34	50−2.58
R_{factor}	0.162	0.164	0.162	0.156
R_{free}	0.195	0.195	0.191	0.192
rmsd[c] for bond lengths (Å)	0.0053	0.0051	0.0126	0.0051
rmsd for bond angles (deg)	1.188	1.147	1.681	1.157
Ramachandran plot (%)				
most favored (disallowed)	92.3 (0.0)	92.2 (0.0)	92.4 (0.0)	92.0 (0.0)
asymmetric unit (no.)				
protein chains	2	4	2	2
herbicide molecules	2	4	2	2
Mg^{2+}	2	4	2	2
K^+	2	4	2	2
ThDP fragments[d]	NSP, YF3, P25, P22	YF1, P25, P22	P23, P22	YF3, YF4, P23
water molecules	1359	2175	1175	912
main chain density				
A	85−263, 284−687	85−269, 277−687	85−270, 278−687	85−269, 277−687
B	85−269, 278−687	86−263, 284−687	85−269, 281−687	85−269, 281−687
C		89−265, 290−687		
D		85−270, 278−687		

[a] Values in parentheses are for the outer resolution shells: 2.19−2.28 Å for CS, 2.29−2.38 Å for MM, 2.34−2.42 Å for SM, and 2.58−2.68 Å for TB. [b] $R_{sym} = \sum|I - \langle I\rangle|/\sum\langle I\rangle$, where I is the intensity of an individual measurement of each reflection and $\langle I\rangle$ is the mean intensity of that reflection. [c] rmsd is the root-mean-square deviation. [d] For SM, only the ethyl and propyl diphosphate fragments could be fitted with certainty, although there was broken density in regions where the pyrimidine and thiazole rings normally sit. For MM, there was broken density in the region where the thiazole ring is normally located, but only the pyrimidine ring and pentyl/ethyl diphosphates could be fitted with certainty.

the asymmetric unit (Table 1), while the MM complex is in space group *I*422 and crystallizes as a tetramer in the asymmetric unit. Thus there are a total of 10 subunit structures, all of which are very similar. For example, the root-mean-square deviations after superimposing all observable Cα atoms between the two subunits in the yeast CE complex and subunits in the CS, MM, TB, and SM complexes range from 0.23 to 0.36 Å. Initially, we will focus our discussion on the CS complex, which has the highest resolution of 2.19 Å. Each subunit consists of three domains (Figure 2A) of approximately equal size, designated α [Asp84 (N-terminus)−Thr277], β (Ser278−Glu464), and γ [Glu465−His687 (C-terminus)]. There are two segments in each subunit where the peptide chain could not be traced. These correspond to the N-terminal hexahistidine tag derived from the expression vector plus the first 26 residues of the mature protein and to a surface polypeptide segment at the boundary of the α- and β-domains (Thr264−Glu283 in subunit A and Ser270−Thr277 in subunit B). Several surface-exposed residues (10 in subunit A and 5 in subunit B) have no observable electron density beyond the β-carbon and were modeled as alanines. Alternative conformations were identified for four side chains in subunit A and nine in subunit B. The three other structures are similar to the CS complex. In all cases, there is a gap in the connection between the α- and β-domains, which ranges in size from 7 to 29 residues; the side chain density is absent for some residues, and alternative conformations were modeled for others. The relative orientations of ThDP, FAD, and CS are shown in Figure 2B.

ThDP Fragmentation. ThDP is not intact in any of the structures; the electron density for the methylaminopyrimidine ring is not connected to that for the diphosphate group, and the thiazolium ring is incomplete. Moreover, it appears that the ThDP fragmentation pattern was not constant through the crystal so that the observed electron density represents an average of different overlapping fragments. For the SM and MM complexes, only the methylaminopyrimidine and diphosphate fragments could be modeled with certainty. For the two other complexes, a reasonable fit between the electron density and a pair of ThDP fragments could be achieved. This is illustrated for the CS complex (subunit B) in Figure 3A. In this example, it appears that the C5−C6 bond is broken, leaving the diphosphate group as its ethyl ester. In addition, the N3−C2 and C2−S1 bonds are broken, releasing C2 and leaving a propane-1-thiol fragment attached to N3. The fragmentation pattern seems to be quite variable, even between subunits within a complex. For example, the two subunits in the CS complex and the two in the TB complex were each best modeled with a different set of fragments.

In the previously determined structure of the CE complex, we reported ThDP fragmentation resulting in the loss of S1 and C2, which we suggested had been caused by synchrotron

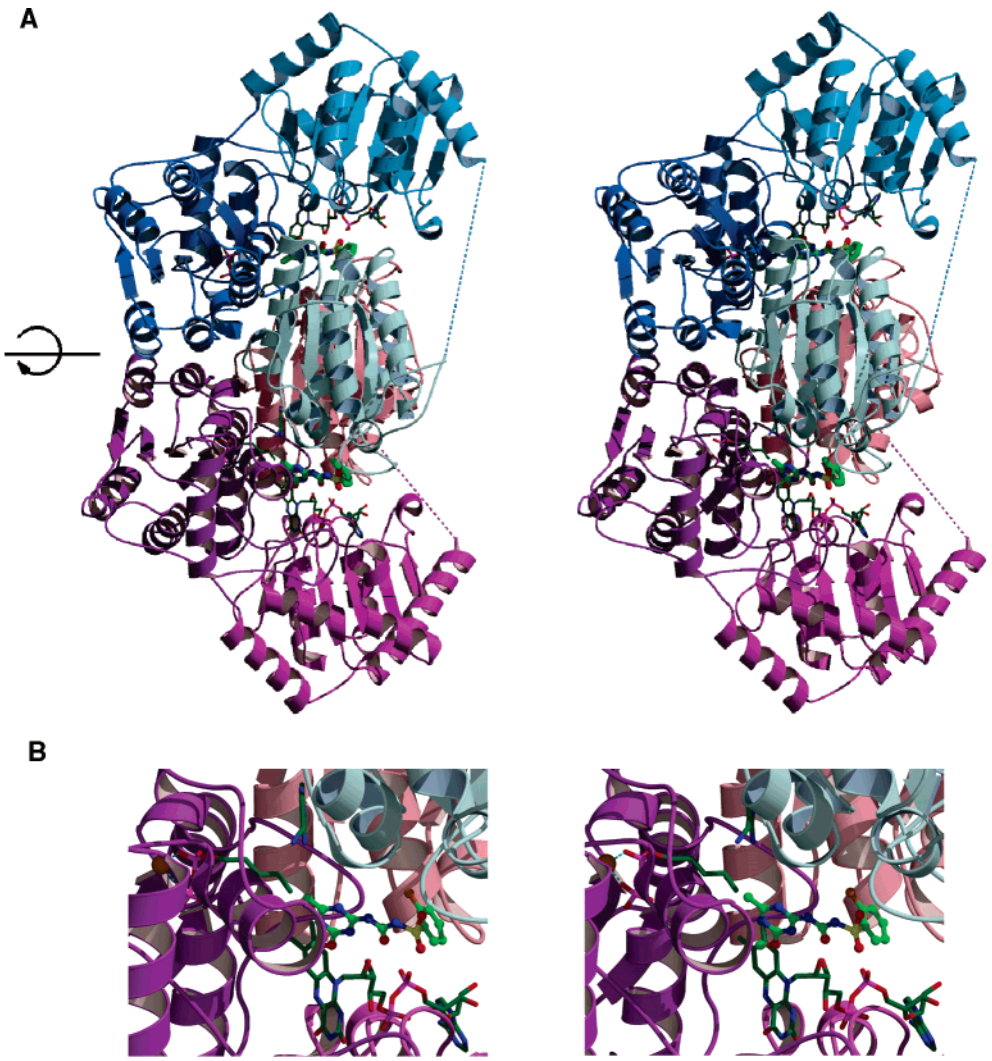

FIGURE 2: (A) Structure of AHAS. Schematic representation of the structure of yeast AHAS in complex with CS. The two subunits are shown in different colors, in three different shades representing the α-domain (light), β-domain (medium), and γ-domain (dark). (B) Magnification of the active site of AHAS. The relative orientations of CS (ball-and-stick model), ThDP (sticks only), Mg^{2+} (brown sphere), and FAD (sticks only) are highlighted.

radiation damage during data collection (*6*). However, we now believe that ThDP is intrinsically unstable when bound to AHAS and some other ThDP-dependent enzymes. Abell and Schloss (*28*) described an oxygenase activity which results from the reactive carbanion intermediate formed midway through the AHAS catalytic cycle. This side reaction generates reactive oxygen species that cause AHAS inactivation. Since the first step of catalysis by ThDP-dependent enzymes involves conversion of the cofactor to its carbanion, it is plausible to propose that ThDP destruction might occur slowly even in the absence of catalysis. These events might only be readily evident after the weeks of incubation needed for protein crystallization. In this context, it may be relevant that ThDP is missing C2 in the crystal structure of *Zymomonas mobilis* pyruvate decarboxylase (*29*). Our previous studies on the structure of AHAS without (*5*) and with (*6*) bound CE have demonstrated closure of the active site when CE is bound. We propose that it is only in this closed state that ThDP can be activated to the carbanion. Herbicide binding triggers active site closure, carbanion formation, and subsequent ThDP degradation.

Conformation of FAD. In the structures of yeast AHAS and its CE complex described previously (*5*, *6*), FAD was modeled with a flat isoalloxazine ring. With the higher-resolution structures that we have now obtained, a bend across the N5−N10 axis is clearly seen. The left half of Figure 4A shows the flat conformation fits poorly into the experimental electron density. On the right of Figure 4A, the isoalloxazine is modeled as the bent conformation observed in pyruvate oxidase [PDB entry 1POX (*12*)]. These data leave little doubt that the isoalloxazine ring is bent, and provide an explanation for the recent observations (*15*, *16*) that FAD can undergo reduction as a side reaction of the catalytic cycle by reacting with the enzyme-bound carbanion/enamine of the hydroxyethyl−ThDP intermediate. The bend across the N5−N10 axis of the ring would increase its redox potential and favor its reduction (*17*).

The extent of bending of the isoalloxazine ring can be quantified by measuring the out-of-plane distances for atoms at the extremities of the molecule. Here we define the plane as consisting of four central atoms in the isoalloxazine ring, namely, C4A, N5, C10, and N10. In subunit A of the yeast AHAS−CS complex, the C7M atom is out of the plane by a distance of 0.66 Å, while for the C8M atom, this distance is 0.85 Å. For O2, this distance is 0.33 Å, and for O4, it is 0.30 Å. Thus, the bend is more pronounced on the dimeth-

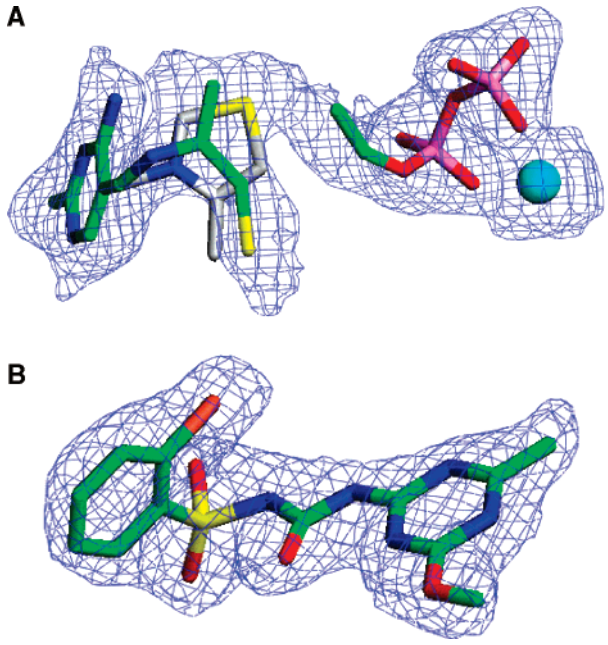

FIGURE 3: (A) ThDP fragments in AHAS. The $F_o - F_c$ omit electron density contoured at 2.0σ is shown for the ThDP fragments in the complex of CS with yeast AHAS (subunit B). Modeled into this structure are the fragments (see Table 1) 2-{[(6-amino-2-methyl-4,5-dihydropyrimidin-5-yl)methyl]amino}propane-1-thiol (left) and ethyl diphosphate (right). The colors represent carbon (green), nitrogen (blue), oxygen (red), phosphorus (pink), and sulfur (yellow). The misfit between the electron density and an intact thiazolium ring is clearly evident; colors are as above, except that carbon is gray. The turquoise sphere is Mg^{2+}. (B) Chlorsulfuron in AHAS. The $F_o - F_c$ omit electron density contoured at 2.0σ is shown for chlorsulfuron in yeast AHAS (subunit A). Colors are as in panel A, with chlorine in orange.

ylbenzene side of the isoalloxazine ring. These distances and distortion biases are typical for all of the complexes observed in this study. Interactions (Figure 4B) can be divided into two types: those that attract atoms of the isoalloxazine ring toward them and those that repel. These interactions, which are very similar across the subunits and the complexes, are listed in Table 2. A comparison of the sequences of 21 AHAS catalytic subunit protein sequences from selected plant, fungal, algal, and bacterial species (*4*) shows that the residues contributing to the bending of the isoalloxazine ring are highly conserved across these species and are usually found in characteristic sequence motifs.

Three of the sulfonylureas make contacts with the isoalloxazine ring, principally through interactions between the methoxy carbon atom at R_2 (Figure 1) of the sulfonylurea and the C7M atom of the isoalloxazine ring. The exception is SM where there are no contacts with the isoalloxazine ring. The reason for this is that SM has only a methyl group at R_2 instead of a methoxy substituent (Figure 1) and therefore is shorter by one atom. It should be emphasized, however, that the interaction between CE, CS, MM, TB, and the isoalloxazine ring of FAD does not contribute to the bending of the ring. Thus, some of the sulfonylureas interact with the isoalloxazine ring, but these contacts are not required for bending.

Herbicides. The channel in which the herbicides are bound leads to the active site and is lined with amino acid side chains that are highly conserved (Table 3). Mutation of most of these residues leads to reduced sensitivity to inhibition by sulfonylureas (*7*, *30*). An $F_o - F_c$ omit map showing the high-quality electron density for CS is presented in Figure 3B. These well-defined features are present for all of the sulfonylureas in this study. The location of CS is illustrated in Figure 5A, and its contacts to the protein are shown in Figure 5B. The vast majority of these contacts are apolar. However, the guanidinium group of Arg380 is hydrogen bonded to the carbonyl oxygen within the sulfonylurea bridge, one of the nitrogen atoms of the heterocyclic ring, and the methoxy oxygen of the R_2 substituent (Figure 1).

The conformation of all of the bound sulfonylureas is very similar (Figure 6), although there are subtle differences, particularly in the location of the aromatic ring and the adjoining sulfonyl oxygen atoms, which lead to some variation in the contacts that each herbicide makes with the protein and nearby water molecules (Figures 5B and 7).

Each of the herbicides makes extensive hydrophobic contacts with the protein (Figures 5B and 7) as well as at least three (one to a nitrogen atom of the heterocyclic ring and two to the carbonyl oxygen of the sulfonylurea bridge) hydrogen bonds to the two terminal side chain nitrogen atoms of Arg380 (Figures 5B and 7). In addition, within at least one subunit of each structure, the oxygen atom of the methoxy substituent on CE, MM, TB, and CS is hydrogen bonded to one of the terminal nitrogens of Arg380, a residue which was recently reported to be crucially important for catalysis (*31*). It is pertinent to note that, with the exception of subunits B and C of the MM-bound structure, only CE is hydrogen bonded to Lys251. This additional contact helps to explain the low K_i value of CE versus other sulfonylureas.

The minimal structure of most active sulfonylureas requires that one ring is an *ortho*-substituted aromatic ring and that the other is a heterocyclic ring. Whether the latter is a pyrimidine ring or a triazine ring seems to be unimportant. Indeed, only one nitrogen atom of this ring (in all of the CE-, CS-, MM-, TB-, and SM-bound AHAS structures) is involved in hydrogen bonding to the protein. In fact, the pyrimidine ring appears to promote tighter binding to the protein through hydrophobic contacts that cannot be made by herbicides bearing a triazine ring (Figures 5B and 7).

The most extensive interactions of all the herbicides are with the indolyl group of Trp586 stacking onto the heterocyclic ring at an average distance of 3.5 Å (Figures 5B and 7). Mutation of Trp586 to leucine will disrupt many of these interactions and has been shown to cause resistance by factors of approximately 10^4 to CS, MM, SM, and TB (*7*). Pro192 and Val583 make similar contacts to all four herbicides, and mutation of these residues affects each herbicide to a similar degree (*7*). Mutation of Gly116 results in several hundred-fold resistance to MM, SM, and TB, while resistance to CS, the only herbicide without direct contacts with this residue, is minimal (5-fold). Despite these correlations between the structures and activities, there are several unexplained anomalies. For example, Ala200 makes almost identical contacts to all four herbicides, but mutation to valine affects inhibition by CS, MM, SM, and TB by factors of 18, 56, 236, and 539, respectively. While these differences are

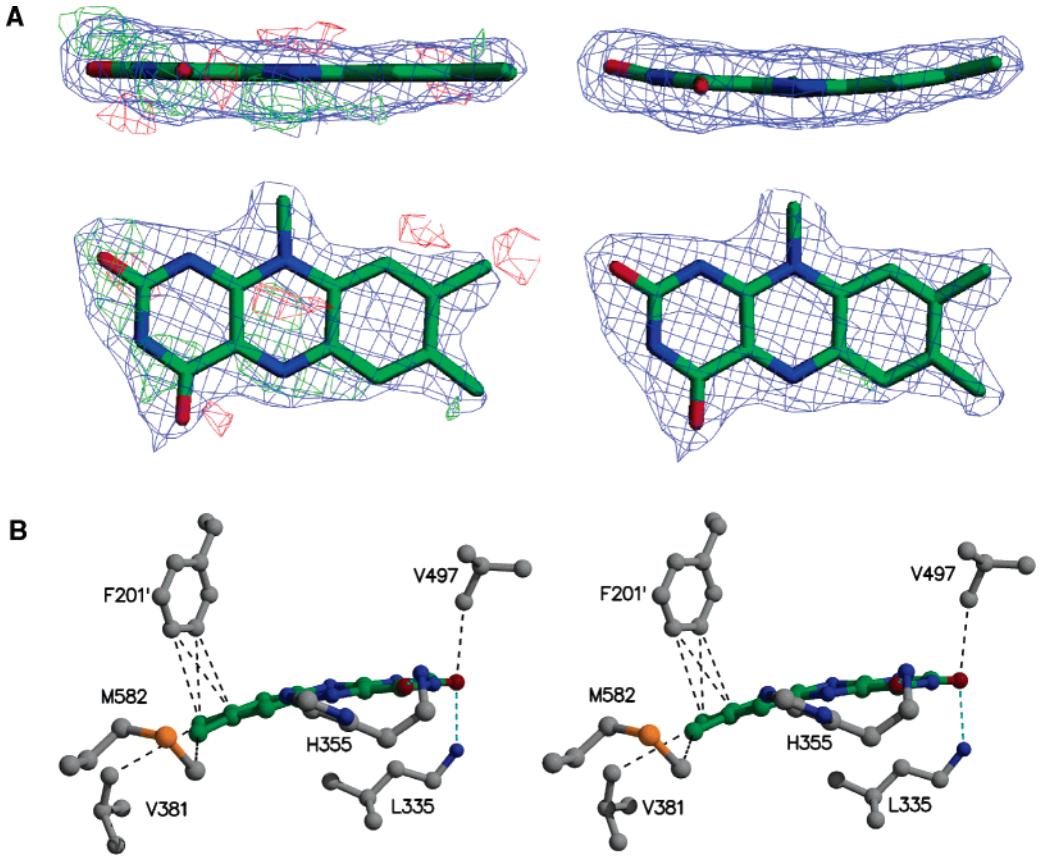

FIGURE 4: (A) Conformation of FAD in AHAS. The $2F_o - F_c$ electron density (contoured at $>1.2\sigma$) before modeling FAD is shown (blue) together with a planar (left) and bent (right) isoalloxazine structure. Green density is contoured at $>2.6\sigma$ and red density at less than -2.6σ. The atom colors represent carbon (green), nitrogen (blue), and oxygen (red). (B) Residues involved in bending the isoalloxazine ring of FAD. The isoalloxazine ring of FAD and the nearby amino acid residues are shown in stereo as ball-and-stick models. Carbon is colored gray in the amino acids and green in the isoalloxazine ring, nitrogen blue, oxygen red, and sulfur orange. Hydrogen bonds and hydrophobic contacts are shown as blue and black dashed lines, respectively.

Table 2: Interactions with AHAS that Favor the Bent Conformation of the FAD Isoalloxazine Ring

residue	FAD atom	type[a]	conserved[b]	sequence[c]
Phe201	C8/C8M	vdW −	21	Asp**AlaPheGlnGlu**
Leu335	O2	H-bond	20	[**Ser/Thr**]Leu*Met*Gly
His355	O4	H-bond	21	**Met***Leu***GlyMetHisGly**
Val381	O2	vdW −	17	**ArgPhe**Asp**AspArg***Val*Thr*Gly*
Val497	C8M	vdW +	21	**ValGlyGln**HisGln**Met**Trp
Met582	C7M	vdW +	20	**Gly**Met**Val**XxxGln**Trp**[**Glu/Gln**]

[a] Interactions are either hydrogen bonds or van der Waals (vdW) interactions, and the latter can favor the bent conformation by either attracting (+) or repelling (−) atoms of the isoalloxazine ring. [b] The number of sequences in which the residue is conserved in the 21 AHAS sequences listed in ref *4*. Of the three other sequences reported in ref *4*, one is known to be an FAD-independent form of the enzyme, while the other two sequences are suspected to be the FAD-independent enzyme. This FAD-independent enzyme exhibits little sequence similarity in these key contact residues. [c] Characteristic sequence motifs containing the contact residues (underlined) are listed. Each residue that is shown is found in at least 18 of the 21 sequences except for those residues shown in italics, which occur 16 or 17 times. Residues shown in bold are conserved in all 21 sequences.

Table 3: Herbicide Contact Residues of AHAS

residue	conserved[a]	closest contact[b]		
Gly116	21	Cα	3.27	N1′
Val191	21	Cγ1	3.53	C6
Pro192	10	Cγ	3.71	O7B
Ala195	3	Cβ	4.42	C5
Ala200	21	Cβ	3.58	C5
Phe201	21	O	3.47	C6
Lys251	21	Cγ	3.70	O7B
Met354	21	Sδ	3.71	O4′
Asp379	21	Oδ	3.30	C5
Arg380	21	NH1	2.98	O9
Met582	20	O	3.61	C7′
Val583	21	Cα	3.78	C7′
Trp586	20	Cζ2	3.33	N3′

[a] The number of sequences in which the residue is conserved in the 21 AHAS sequences listed in ref *4*. [b] Closest distances are shown as amino acid atom, distance in angstroms, and CS atom.

striking, they represent at most a change in the relative binding energy of 8.6 kJ/mol, which could be explained by a difference of a single van der Waals contact. Interpreting data from a mutated protein using a wild-type structure is not straightforward, as illustrated by Ala117 and Phe590. Neither residue makes any contacts with these sulfonylureas, but mutation of each results in resistance. Presumably, these mutations affect the positions of other residues (e.g., Gly116 and Trp586) and impart herbicide resistance indirectly.

When Connolly surfaces (results not shown) are calculated for the herbicide-binding site in all five structures, it is obvious why these herbicides are excellent inhibitors of AHAS. The aromatic ring might be capable of slight side-to-side movement, but the sulfonylurea bridge fits snugly into the surrounding pocket. There is room only for the *ortho* substituent of the aromatic ring (which lies parallel to the sulfonylurea bridge) and surrounding water molecules.

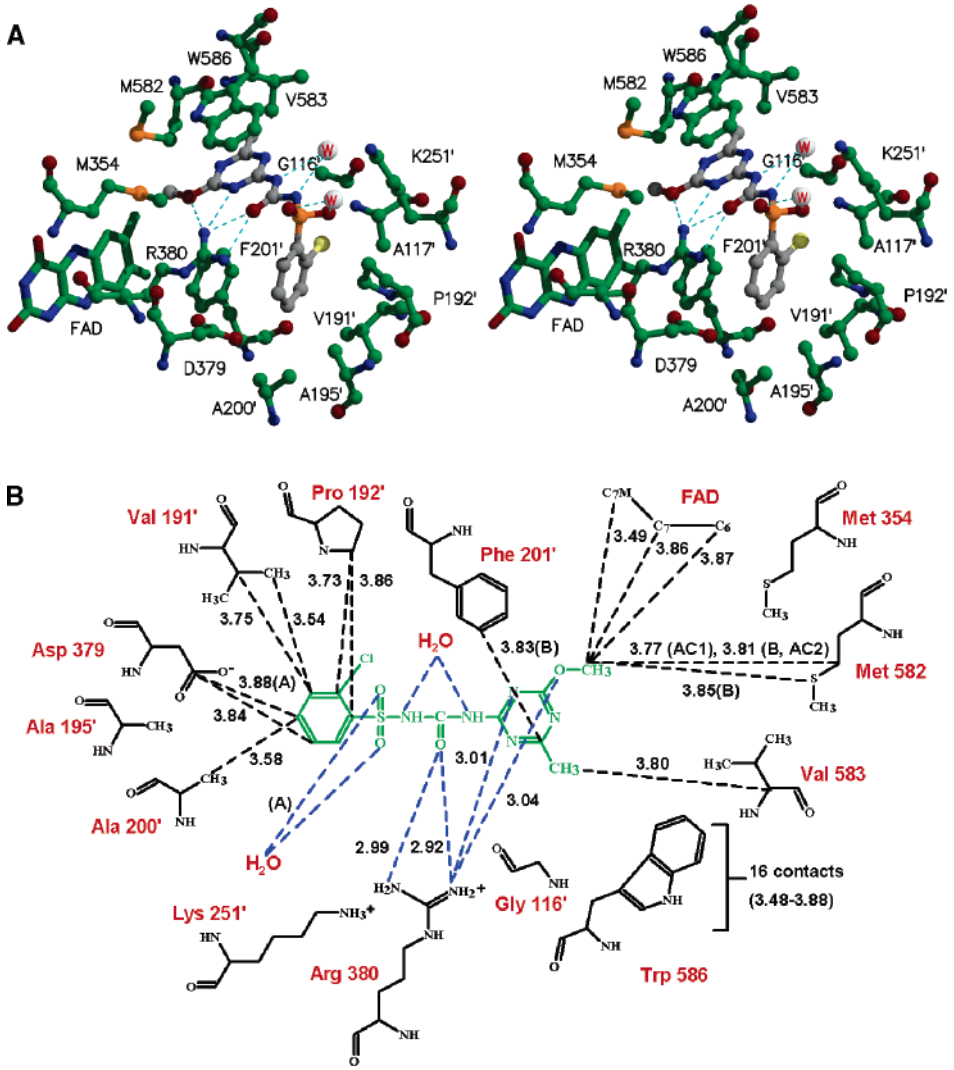

FIGURE 5: CS in the herbicide binding site of AHAS. (A) The herbicide and nearby amino acids are shown as ball-and-stick models. The atom colors represent carbon (green, amino acids; gray, CS), nitrogen (blue), oxygen (red), sulfur (orange), and chlorine (yellow). The isoalloxazine ring of FAD is shown as a stick model. Hydrogen bonds are drawn as dashed lines, and water molecules are identified by solid spheres with a red W. (B) Distances in angstroms from CS are indicated with broken lines for hydrophobic contacts (black) and hydrogen bonds (blue). Distance cutoffs of 3.2 and 3.9 Å were employed for hydrogen bond and van der Waals interactions, respectively.

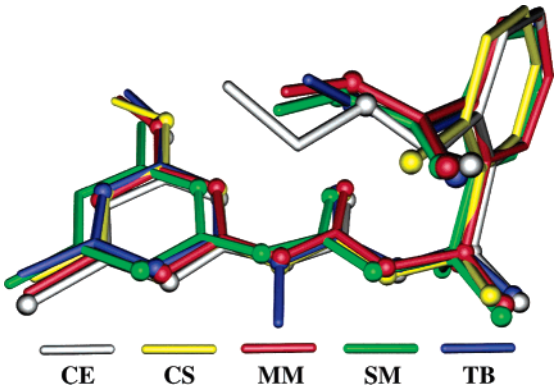

FIGURE 6: Overlay of sulfonylurea structures. The five yeast AHAS polypeptides (taken from complexes) were superimposed to reveal the relative orientations of the sulfonylurea herbicides. The structure of CE is from previously published data (*6*), while those of the remaining sulfonylureas are reported here. To assist in orienting the structures, all non-carbon atoms (nitrogen, oxygen, sulfur, and chlorine) are shown as spheres.

Herbicides bearing either an ethyl ester (CE) or a smaller methyl ester (MM, SM, or TB) substituent on the aromatic ring complement the protein nicely, whereas the much smaller chlorine in CS does not fit tightly into the surrounding space. Thus, the difference in K_i values for these inhibitors can at least be partly attributed to the size of this group; CE and MM inhibit yeast AHAS with K_i values of 3.25 and 9.40 nM, respectively, while that for CS is 127 nM (*7*). The heterocyclic ring binding region has room on one side for a relatively small methyl group (MM, SM, TB, and CS) or a chlorine atom (CE), whereas the other *meta* position protrudes into the space surrounding the isoalloxazine ring of FAD and can accommodate the somewhat larger methoxy substituent on CE, CS, TB, and MM.

Conservation of the Herbicide Binding Site. Eleven of the 13 residues that make contact with the sulfonylureas (Figures 5B and 7) are conserved to an astonishing degree across plant, fungal, and bacterial AHAS sequences (Table 3); Met582 and Trp586 are replaced in the *Escherichia coli* AHAS I sequence only. This high degree of conservation points to important roles for these amino acids in the AHAS reaction, and in some cases, there is supporting experimental

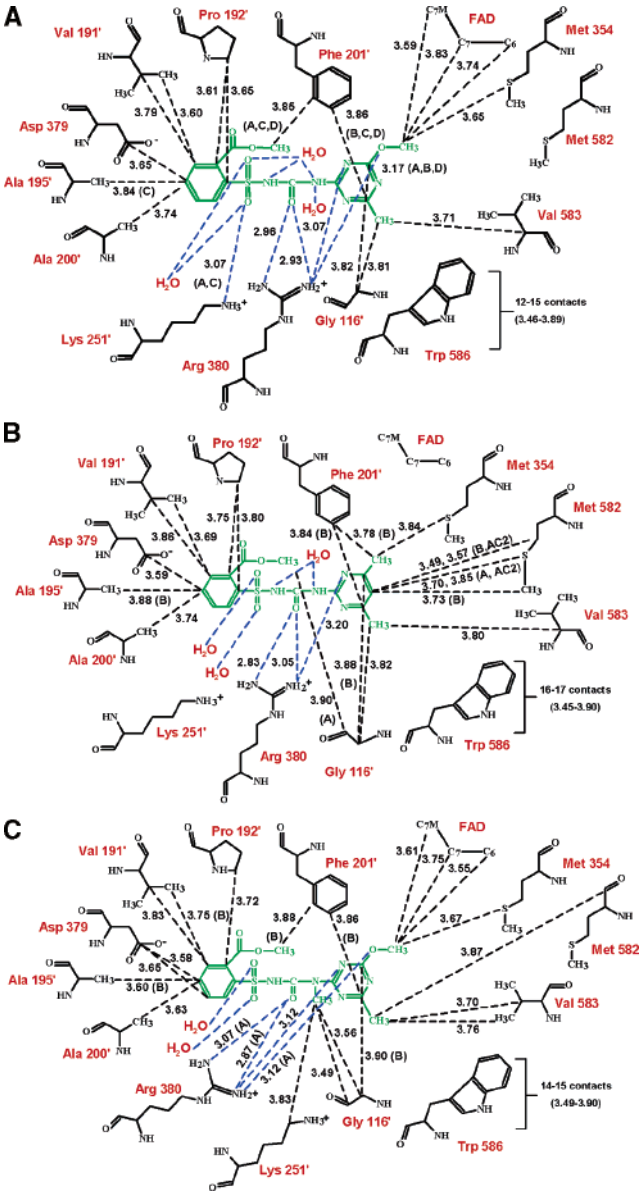

FIGURE 7: Contacts with sulfonylureas in the herbicide binding site of AHAS. Distances in angstroms from MM (A), SM (B), and TB (C) are indicated with dashed black lines for hydrophobic contacts and dashed blue lines for hydrogen bonds. Distances and limits are as described in the legend of Figure 5.

evidence. Mutations of the equivalent residues to Arg380 and Phe201 in *E. coli* AHAS II cause decreases in activity (*31*), but in other cases, their effects on activity may be more subtle. Thus, mutations at Trp586 in yeast AHAS (*7*), *Arabidopsis thaliana* AHAS (*32*), or *E. coli* AHAS II (*31*), yield an enzyme with high activity but (in the case of *E. coli* AHAS II) with a greatly decreased preference for 2-ketobutryate as the second substrate. Thus, this tryptophan plays a role in substrate recognition, and it is relevant that *E. coli* AHAS I shows sequence variation at Trp586 observed in no other AHAS (Table 3), and has a low preference for 2-ketobutryate.

CONCLUSIONS

In summary, the isoalloxazine ring of FAD adopts a bent conformation in AHAS which is indistinguishable from that of POX. Thus, this structural study supports the recent finding that AHAS is capable of reducing FAD as a minor side reaction (*15*, *16*). The five herbicides, CE, CS, MM, TB, and SM, all inhibit yeast AHAS by a similar mechanism, principally by forming strong interactions between amino acid side chains dispersed along the length of the protein. The structures highlight the high degree of complementarity between the binding sites and the molecular envelope provided by these inhibitors. The common contacts contribute to the overall low K_i values of these sulfonylurea herbicides. It is now possible to rationalize some of the more subtle structural variations in terms of the K_i data.

ACKNOWLEDGMENT

We thank Harry Tong and Keith Brister for assistance with data collection at the Advanced Photon Source.

REFERENCES

1. Sauers, R. F., and Levitt, G. (1984) Sulfonylureas: New high potency herbicides, in *Pesticide Synthesis Through Rational Approaches* (Magee, P. S., Kohn, G. K., and Menn, J. J., Eds.) pp 21−28, American Chemical Society, Washington, DC.
2. LaRossa, R. A., and Schloss, J. V. (1984) The sulfonylurea herbicide sulfometuron methyl is an extremely potent and selective inhibitor of acetolactate synthase in *Salmonella typhimurium*, *J. Biol. Chem. 259*, 8753−8757.
3. Ray, T. B. (1984) Site of action of chlorsulfuron: inhibition of valine and isoleucine biosynthesis of plants, *Plant Physiol. 75*, 827−831.
4. Duggleby, R. G., and Pang, S. S. (2000) Acetohydroxyacid synthase, *J. Biochem. Mol. Biol. 33*, 1−36.
5. Pang, S. S., Duggleby, R. G., and Guddat, L. W. (2002) Crystal structure of yeast acetohydroxyacid synthase: a target for herbicidal inhibitors, *J. Mol. Biol. 317*, 249−262.
6. Pang, S. S., Guddat, L. W., and Duggleby, R. G. (2003) Molecular basis of sulfonylurea herbicide inhibition of acetohydroxyacid synthase, *J. Biol. Chem. 278*, 7639−7644.
7. Duggleby, R. G., Pang, S. S., Yu, H., and Guddat, L. W. (2003) Systematic characterization of mutations in yeast acetohydroxyacid synthase: Interpretation of herbicide-resistance data, *Eur. J. Biochem. 270*, 2895−2904.
8. Störmer, F. C., and Umbarger, H. E. (1964) The requirement for flavin adenine dinucleotide in the formation of acetolactate by *Salmonella typhimurium* extracts, *Biochem. Biophys. Res. Commun. 17*, 587−592.
9. Störmer, F. C. (1968) The pH 6 acetolactate-forming enzyme from *Aerobacter aerogenes*. II. Evidence that it is not a flavoprotein, *J. Biol. Chem. 243*, 3740−3741.
10. Chang, Y.-Y., and Cronan, J. E., Jr. (1988) Common ancestry of *Escherichia coli* pyruvate oxidase and the acetohydroxy acid synthases of the branched-chain amino acid biosynthetic pathway, *J. Bacteriol. 170*, 3937−3945.
11. Schloss, J. V., Ciskanik, L. M., and Van Dyk, D. E. (1988) Origin of the herbicide binding site of acetolactate synthase, *Nature 331*, 360−362.
12. Muller, Y. A., Schumacher, G., Rudolph, R., and Schulz, G. E. (1994) The refined structures of a stabilized mutant and of wild-type pyruvate oxidase from *Lactobacillus plantarum*, *J. Mol. Biol. 237*, 315−335.
13. Pang, S. S., Duggleby, R. G., Schowen, R. L., and Guddat, L. W. (2004) The crystal structures of *Klebsiella pneumoniae* acetolactate synthase with enzyme-bound cofactor and with an unusual intermediate, *J. Biol. Chem. 279*, 2242−2253.
14. Schloss, J. V., and Aulabaugh, A. (1988) Acetolactate synthase and ketol-acid reductoisomerase: A search for a reason and a reason for a search, in *Biosynthesis of Branched Chain Amino Acids* (Barak, Z., Chipman, D. M., and Schloss, J. V., Eds.) pp 329−356, VCH Press, Weinheim, Germany.
15. McCourt, J. A. (2004) Structural and mechanistic studies on acetohydroxyacid synthase and related enzymes, Ph.D. Thesis, The University of Queensland, Brisbane, Australia.
16. Tittmann, K., Schröder, K., Golbik, R., McCourt, J., Kaplun, A., Duggleby, R. G., Barak, Z., Chipman, D., and Hübner, G. (2004) Electron transfer in acetohydroxy acid synthase as a side reaction

of catalysis. Implications for the reactivity and partitioning of the carbanion/enamine form of α-hydroxyethylthiamin diphosphate in a "nonredox" flavoenzyme, *Biochemistry 43*, 8652−8661.
17. Muller, Y. A., and Schulz, G. E. (1993) Structure of the thiamin- and-flavin-dependent enzyme pyruvate oxidase, *Science 259*, 965−967.
18. Pang, S. S., and Duggleby, R. G. (1999) Expression, purification, characterization and reconstitution of the large and small subunits of yeast acetohydroxyacid synthase, *Biochemistry 38*, 5222−5231.
19. Lee, Y.-T., and Duggleby, R. G. (2002) Regulatory interactions in *Arabidopsis thaliana* acetohydroxyacid synthase, *FEBS Lett. 512*, 180−184.
20. Smith, P. K., Krohn, R. I., Hermanson, A. K., Gartner, F. H., Provenzano, M. D., Fujimoto, E. K., Goeko, N. M., Olsen, B. J., and Klenk, D. C. (1985) Measurement of protein using bicinchoninic acid, *Anal. Biochem. 150*, 76−85.
21. Otwinowski, Z., and Minor, W. (1997) Processing of X-ray diffraction data collected in oscillation mode, *Methods Enzymol. 276*, 307−326.
22. Navaza, J. (1994) AMoRe: An automated package for molecular replacement, *Acta Crystallogr. A50*, 157−163.
23. Brünger, A. T., Adams, P. D., Clore, G. M., Delano, W. L., Gros, P., Grosse-Kunstleve, R. W., et al. (1998) Crystallography and NMR system (CNS): A new software system for macromolecular structure determination, *Acta Crystallogr. D54*, 905−921.
24. Jones, T. A., Zou, J. Y., Cowan, S. W., and Kjeldgaard, M. (1991) Improved methods for building protein models in electron density maps and the location of errors in these models, *Acta Crystallogr. A47*, 110−119.
25. Evans, S. V. (1993) SETOR: Hardware lighted three-dimensional solid model representations of macromolecules, *J. Mol. Graphics 11*, 134−138.
26. Kraulis, P. J. (1991) MOLSCRIPT: A program to produce both detailed and schematic plots of protein structures, *J. Appl. Crystallogr. 24*, 946−950.
27. Merritt, E. A., and Bacon, D. J. (1997) RASTER3D: Photorealistic molecular graphics, *Methods Enzymol. 277*, 505−524.
28. Abell, L. M., and Schloss, J. V. (1991) Oxygenase side reactions of acetolactate synthase and other carbanion-forming enzymes, *Biochemistry 30*, 7883−7887.
29. Dobritzsch, D., König, S., Schneider, G., and Lu, G. (1998) High-resolution crystal structure of pyruvate decarboxylase from *Zymomonas mobilis*. Implications for substrate activation in pyruvate decarboxylases, *J. Biol. Chem. 273*, 20196−20204.
30. Falco, S. C., McDevitt, R. E., Chui, C.-F., Hartnett, M. E., Knowlton, S., Mauvais, C. J., Smith, J. K., and Mazur, B. J. (1989) Engineering herbicide-resistant acetolactate synthase, *Dev. Ind. Microbiol. 30*, 187−194.
31. Engel, S., Vyamensky, M., Vinogradov, M., Berkovich, D., Bar-Ilan, A., Qimron, U., Rosiansky, Y., Barak, Z., and Chipman, D. (2004) Role of a conserved arginine in the mechanism of acetohydroxyacid synthase, *J. Biol. Chem. 279*, 24803−24812.
32. Chang, A. K., and Duggleby, R. G. (1998) Herbicide-resistant forms of *Arabidopsis thaliana* acetohydroxyacid synthase: Characterization of the catalytic properties and sensitivity to inhibitors of four defined mutants, *Biochem. J. 333*, 765−777.

BI047980A